



ELSEVIER

Available online at [www.sciencedirect.com](http://www.sciencedirect.com)

SCIENCE @ DIRECT®

Electronic Notes in Discrete Mathematics 20 (2005) 133–150

Electronic Notes in  
DISCRETE  
MATHEMATICS

[www.elsevier.com/locate/ndm](http://www.elsevier.com/locate/ndm)

# Quantum Tomography for Imaging

Giacomo Mauro D’Ariano<sup>1,2</sup> and Lorenzo Maccone<sup>3</sup>

*QUIT - Quantum Information Theory Group, Dip. di Fisica “A. Volta”,  
Università di Pavia, via A. Bassi 6, I-27100 Pavia, ITALY<sup>4,5</sup>*

---

## Abstract

We present a method to perform tomographic imaging starting from very little data. The reconstruction of arbitrary images is performed using techniques mutuated from quantum state reconstruction. Almost maximal information gain from each datum is achieved, yielding a reduction in the radiation exposure of the imaged sample.

*Keywords:* Tomography, imaging, quantum mechanics, quantum tomography.

---

Cross-pollination of different fields is often a difficult albeit fruitful endeavor. Here we connect the fields of quantum tomography and of tomographic imaging. Our findings seem to indicate that, using available hardware, CT-scans might be achieved with lower irradiation levels. Apart from the name (which in the quantum setting is dictated solely by historical reasons), these two fields seem completely disconnected. However, quantum fluctuations are the main sources of noise in CT-scans with low intensity [15], so that it might not be too surprising that a quantum technique may provide good enhancements.

---

<sup>1</sup> Also: *Center for Photonic Communication and Computing*, Department of Electrical and Computer Engineering, Northwestern University, Evanston, IL 60208

<sup>2</sup> Email: [dariano@unipv.it](mailto:dariano@unipv.it)

<sup>3</sup> Email: [maccone@unipv.it](mailto:maccone@unipv.it)

<sup>4</sup> URL: [www.qubit.it](http://www.qubit.it)

<sup>5</sup> URL: [www.quantummechanics.it](http://www.quantummechanics.it)

Quantum state reconstruction [10], or *quantum tomography* (QT), is a set of methods that allow one to obtain the quantum state of a physical system (i.e. a matrix or an operator) starting from a set of measurements on identically prepared systems. This operator, the so-called density operator or density matrix, contains the whole information available on the system. Quantum complementarity (of which wave-particle duality is a well known aspect) forbids to obtain all the possible information from the same measurement: if we are measuring the wave aspects of the systems, we are missing out on all its particle aspects. Thus, to recover the state, we need to perform a set of different measures. For example, to recover the quantum state of a harmonic oscillator, we need to measure its position  $Q$ , its momentum  $P$ , and all linear combinations of position and momentum—the so-called *quadratures* of the oscillator— $X_\phi = Q \cos \phi + P \sin \phi$ , parametrized by the angle  $0 \leq \phi \leq \pi$ .

Computerized tomography (CT), on the other hand, is a procedure where multiple one-dimensional projections of an object (i.e. intensity profiles) taken from different angles around a single axis of rotation are combined to yield a two-dimensional image of the object. Usually this is achieved using the mathematical procedure called inverse Radon transform [3,16]. Analogously to the quantum case, a single measurement, yielding the intensity profile along a single direction, is insufficient to recover the whole image.

The two procedures QT and CT have a unifying trait. The quantum state of a harmonic oscillator can be represented by a two-variable function, the Wigner function, in phase space. Its projection (i.e. its marginal integral) along the direction in phase space indicated by  $\phi$  establishes the probability distribution that governs the measurement of the corresponding quadrature  $X_\phi$  (see Fig. 1). The first quantum tomographic method [19] exploited this property to recover the Wigner function (and thus the state) via an inverse Radon transform from the quadrature probability distributions. Subsequent methods [10] achieve a much higher level of refinement, and are able to recover the density matrix directly from the single measurement outcomes. In this way, two important problems connected with the Radon transform inversion are avoided. First, the density matrix obtained from a numerically evaluated Wigner function may present severe artifacts due to the complicated relation that connects the two quantities (see Sec. 2). Second, there is no need to recover the quadrature probability distributions, i. e. the marginals of the Wigner functions. This would entail binning the measurement outcomes to recover the probability from a histogram, and there is, of course, a tradeoff between bin width and accuracy of the estimated probability. The estimation will be accurate only in the limit of infinite data points (see Fig. 2b). The

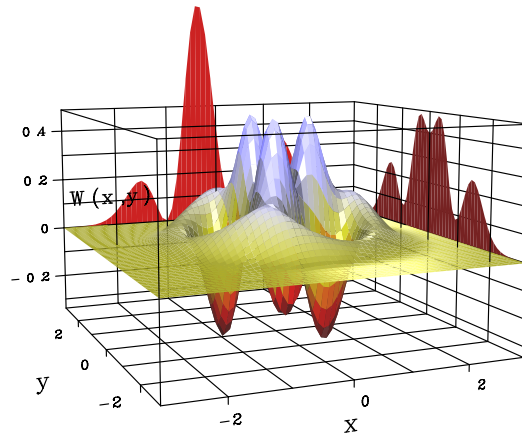


Fig. 1. Marginal distributions (dark functions plotted on the axes) of a Wigner function (the two-variables function in the center). The marginals are obtained by integrating the Wigner function in the orthogonal direction (i.e. along the  $x$  axis for the marginal plotted on the  $y$  axis and along the  $y$  axis for the marginal plotted on the  $x$  axis). [In particular, this Wigner function refers to the state  $\frac{1}{\sqrt{2}}(|0\rangle + |3\rangle)$  (i.e. an equal superposition of the two Fock states  $|0\rangle$  and  $|3\rangle$ )]

first of these problems has no interest in tomographic imaging, but the second is crucial: if the sample is irradiated with a too low radiation intensity, the resulting one-dimensional intensity profiles present a granular structure due to the occurrence of single photon events [15]. This means that the intensity profile is dominated by statical fluctuations of quantum origin, which will appear also in the tomogram. Even though various smoothing techniques are known and routinely employed, it seems logically preferable to bypass the use of the inverse Radon transform (which requires the intensity profiles as inputs), and use a procedure that employs singularly each of the data points.

In this paper, following the lines of Ref. [8], we propose a method to realize this goal, by extending the methods of quantum state reconstruction to the field of tomographic imaging. Instead of the averaged intensity profiles, our algorithm employs separately each single detected photon. A couple of free parameters allow for the fine tuning of the output image quality. As an intermediate step of the procedure we find the “density matrix” associated with the image we are seeking. Analogously to the quantum case, this matrix contains all the information that can be extracted from the given intensity profiles. Even though in this case it has no physical interpretation, it may still be viewed as a convenient method of storing the acquired data. An

added bonus of our method is that the density matrix is obtained by averaging the data: thus one can monitor in real time the output image and stop the irradiation when sufficient detail is reached. There is no need to acquire all the data prior to the reconstruction, as in some of the conventional methods. Moreover, thanks to the algorithm's linearity, it can be easily parallelized allowing several processors to concurrently work at the same reconstruction.

Our method can be applied not only to obtain CT-scans with much less radiation doses, but also to improve the quality of the reconstruction in imaging fields where only very few events naturally occur, such as in Positron Emission Tomography (PET) or in Single Photon Emission Computed Tomography (SPECT).

In Sec. 1 we start by describing the procedure we propose and the experimental apparatus which is needed. Some Monte-Carlo simulations of our procedure are presented together with a rough analysis of the required radiation doses. In Sec. 2 we give the detailed derivation of the inversion relations involved, introducing as little quantum mechanical concepts as possible. In Sec. 3 we analyze various possible refinements that might be brought into our method, borrowed from quantum state reconstruction procedures.

## 1 Quantized-CT

In this section we present the Quantized-Computer-Tomography (QCT) method that allows for good tomographic reconstructions even with very few photons.

At the input, QCT needs a set of  $N$  data points  $\{(\phi_k, x_k)\}$  with  $k = 1, \dots, N$ , where  $\phi_k$  is the angle of the source beam when the  $k$ th event was measured and  $x_k$  is the position (in a plane orthogonal to the beam direction) where the photon was absorbed (see Fig. 2a). This information can be easily obtained from the circular detector array geometry conventionally used in CT scanners or PET arrangements (see Fig. 2a). In the following we will assume that the incoming light is in a plane wave configuration; different illuminations can be easily accounted for with appropriate transformations on the reconstructed image.

While the data is being picked up from the detector array, it can be immediately fed into the algorithm to recover the density matrix elements  $\rho_{nm}$ . The algorithm consists in performing the following average using the  $N$  data

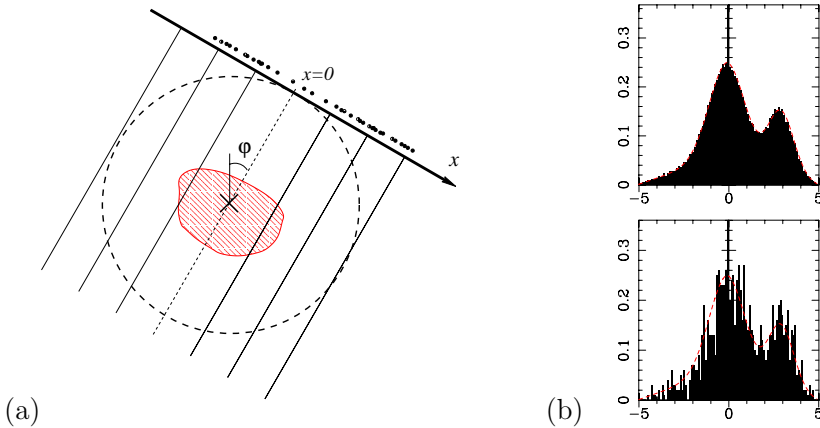


Fig. 2. (a) Geometrical meaning of the parameters  $\phi$  and  $x$ . The central cross is the axis of rotation of the incoming beam, deflected by an angle  $\phi$  with respect to a fixed reference. The thick upper line is the detector array, where the coordinate  $x$  measures the photon arrival positions (represented by small dots). If the detector arrays are arranged in a circle (with an angular coordinate  $\theta$  indicating the detector that fired), it is clear from the picture that the  $x$  coordinate can be recovered as  $x \propto \tan(\theta - \phi)$ . (b) Illustrative example of the statistical fluctuations that are encountered when recovering the intensity profiles from the data through histograms. In the upper graph  $10^5$  data points are distributed into 100 histogram bins: the fluctuations are almost negligible; in the lower graph we have only  $10^3$  data points distributed into 100 histogram bins: the fluctuations are evident.

points  $\{(\phi_k, x_k)\}$  [6]:

$$(1) \quad \varrho_{nm} = \frac{1}{N} \sum_{k=1}^N K_{nm}(\phi_k, x_k) ,$$

where the function  $K_{nm}$  (called kernel function) is given by

$$(2) \quad K_{nm}(\phi, x) \equiv 2e^{i(n-m)\phi} \sqrt{\frac{n!}{m!}} e^{-x^2} \sum_{j=n-m}^n \frac{(-1)^j}{j!} \binom{m}{n-j} \times (2j + m - n + 1)! \text{Re} [(-i)^{m-n} \mathcal{D}_{-(2j+m-n+2)}(-2ix)] ,$$

where  $\mathcal{D}_l(x)$  denotes the parabolic cylinder function and  $\text{Re}$  denotes the real part. The apparently complicated expression of Eq. (2) can be easily calculated numerically through the recursion relations of the parabolic cylinder functions [11]. [Instead of the expression (2), it is advisable to employ the recursive procedure outlined in the appendix, which is numerically fast and more stable, since  $K_{nm}$  is there factorized into a product of two vectors which

depend only on  $n$  and  $m$  respectively]. Thanks to linearity of Eq. (1), the algorithm can be easily parallelized: assign a portion of the data points to each cpu, and then take the average of the density matrices obtained by each of them.<sup>6</sup> Since we are dealing with the harmonic oscillator (see Sec. 2), ideally we would need to recover an infinite-dimensional matrix  $\varrho$ . Naturally, we are limited to reconstructing a finite dimensional  $M \times M$  matrix (with the indices  $n$  and  $m$  taking the values  $0, \dots, M - 1$ ).

The average in Eq. (1) allows us to recover the density matrix  $\varrho$  from the input data. Before seeing how to recover the image from the density matrix  $\varrho$ , let us analyze the effect of the cutoff parameter  $M$ . Any image can be put into a one-to-one relation with its “density matrix”  $\varrho$  through the formulas that will be analyzed in the following section. If we limit the matrix to an  $M \times M$  submatrix, we are losing some information (see Fig. 3). However, the reconstruction of the matrix elements with high index values  $n$  and  $m$  requires more data, since they refer to rare events with high “harmonic oscillator excitation number”. Correspondingly, the functions  $K_{nm}(\phi, x)$  oscillate more rapidly as a function of  $x$  for larger  $n$  and  $m$ . Thus, in practice, it is advantageous to perform a cutoff when the number of data is limited, since it cancels the statistical fluctuations in the matrix elements  $\varrho_{nm}$  for high  $n, m$ . This increases the image quality in practice, even though in theory we are losing some detail: however, the increase in resolution corresponding to increasing the cutoff  $M$  would be washed out by the statistical fluctuations in the high-index-value elements of  $\varrho$ . Thus, the cutoff  $M$  can be used as a tuning parameter to increase the quality of the image for a given set of data. It is difficult to estimate *a priori* the optimal value of  $M$  since it depends on the image to be recovered. A simple image (with few high resolution details) might be well described by a small density matrix. [In the examples given in the figures, the apple logo is encoded quite nicely into a  $50 \times 50$  matrix, while the brain slice needs at least a  $300 \times 300$  matrix].

Once the density matrix has been obtained through the average of Eq. (1), the image  $W(r, \phi)$ , expressed in radial coordinates  $r$  and  $\phi$ , can be accessed via

$$(3) \quad W(r, \phi) = \text{Re} \left[ \sum_{n=0}^{M-1} \sum_{d=0}^{M-1-n} e^{i\phi d} \Lambda(n, d; \gamma r) \varrho_{n, n+d} \right],$$

---

<sup>6</sup> The alternative parallelizing strategy of assigning a matrix element to each computer seems not convenient, since it can hardly exploit the power of the recursion relations in the calculation of the kernel functions and since all processors must be furnished with the whole data set.

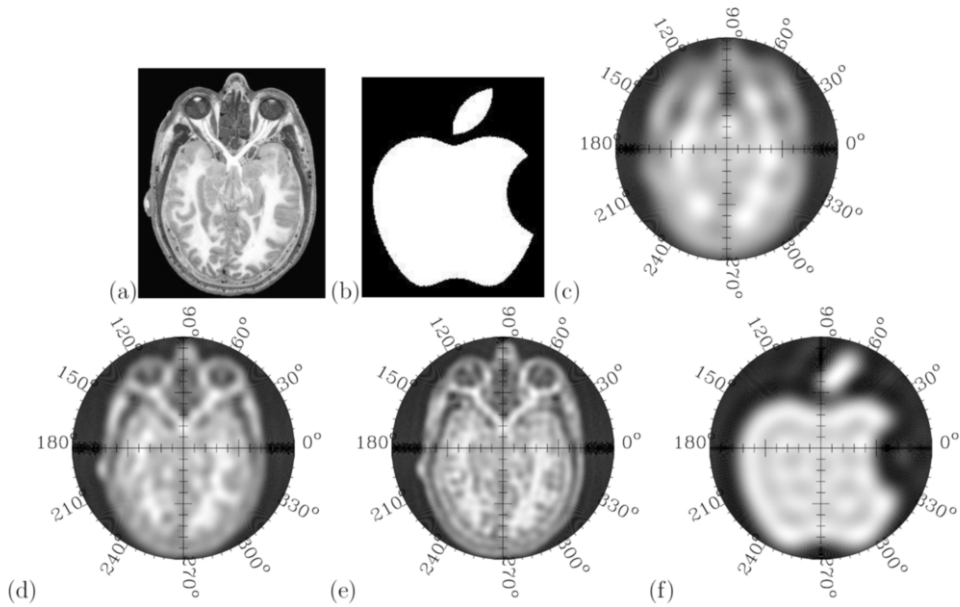


Fig. 3. Effect of the density matrix truncation parameter  $M$ . (a) and (b) Photograph of a head slice and the apple-logo that have been used as starting points for the simulations. (c) Image obtained by recovering numerically the  $\varrho$  relative to the image in (a) through Eq. (11) and then back to the image through (10). Here the cutoff parameter is  $M = 30$ . (d) Same as the previous, with cutoff parameter  $M = 150$ . (e) Same as the previous, with cutoff parameter  $M = 300$ . Notice the increase in detail for increasing  $M$ . (f) Same as the previous, using the image (b), with  $M = 40$ : for simple images a low cutoff parameter is sufficient to recover most details.

where  $\gamma$  is a positive scale parameter and

$$(4) \quad \Lambda(n, d; r) \equiv (-1)^n 2(2 - \delta_{d0})(2r)^d \sqrt{\frac{n!}{(n+d)!}} e^{-2r^2} L_n^d(4r^2),$$

where  $\delta_{jk}$  is the Kronecker delta and  $L_n^d$  is the generalized Laguerre polynomial. As before, the expression (4) can be easily calculated from the appropriate recursion relations [11]. The scale parameter  $\gamma$  follows from the fact that one can choose arbitrarily the width of the image pixels. In the quantum mechanical derivation the  $\gamma$  factor is fixed to  $\gamma = 1$  (here the scale is dictated

by the value of commutator between complementary observables, i. e. by the Planck constant). Examples of reconstructions are given in Fig. 4, where the whole QCT procedure has been simulated using Monte-Carlo techniques. The simulated data points have phases  $\phi$  uniformly-random distributed in the interval  $[0, \pi]$ . (In usual CT phases are uniformly scanned, collecting more photons for each phase with the X-ray source fixed. In QT if uniform phase scanning is used, the optimal number of phases equals the cutoff parameter  $M$  [13].)

### 1.1 Dosimetry analysis of the method

As anticipated above, the main advantage of our scheme over conventional tomographic reconstruction mechanisms consists in a lower necessary dose of radiation. Here we give a brief analysis with some real-life examples.

An average CT scan of a slice of human head entails an absorbed radiation dose of around 50 mGy [18]. Assuming a slice thickness of 5 mm and a diameter of 15 cm with the density of water, we find a mass of around 100 g. This means that the energy absorbed by the slice during the scan is  $E \simeq 5$  mJ. A field of 120 KV is typically used in CT scans, and it produces a spectrum of photons peaked around an energy-per-photon of  $E_{pp} = 60$  KeV [18,12]. Thus, the number of photons absorbed during the scan is on the order of  $N = E/E_{pp} \simeq 5.2 \times 10^{11}$ . Assuming 1.5 cm of compact bone and 14 cm of muscle, we find around 5 half-value-layers (i.e. tissue lengths that absorb half of the incoming radiation) [17]: it corresponds to an absorption of  $\gamma \simeq 97\%$  of the incoming energy. Thus, the number of photons which reach the detectors are about  $N(1 - \gamma)/\gamma \simeq 1.7 \times 10^{10}$ . Our simulations show that good quality images (see Fig. 4a) can be obtained from around  $5 \times 10^7$  events, with a reduction of the irradiation of around 350 times for a CT-scan with the same quality of the one given in Fig. 4a. We want to emphasize that this is not the optimum achievable with QCT (see Sect. 8).

## 2 Mathematical details and inverse transformation

In this section we derive the reconstruction formulas introduced above. The main idea is to transfer the quantum-state-reconstruction methods to imaging. If we consider a harmonic oscillator, its quantum state is described by a Wigner function, whose marginal projections are the probability distributions of quadrature measurement results. We can, thus, interpret the tomogram as a Wigner function, and then use the tomographic data as if it was coming

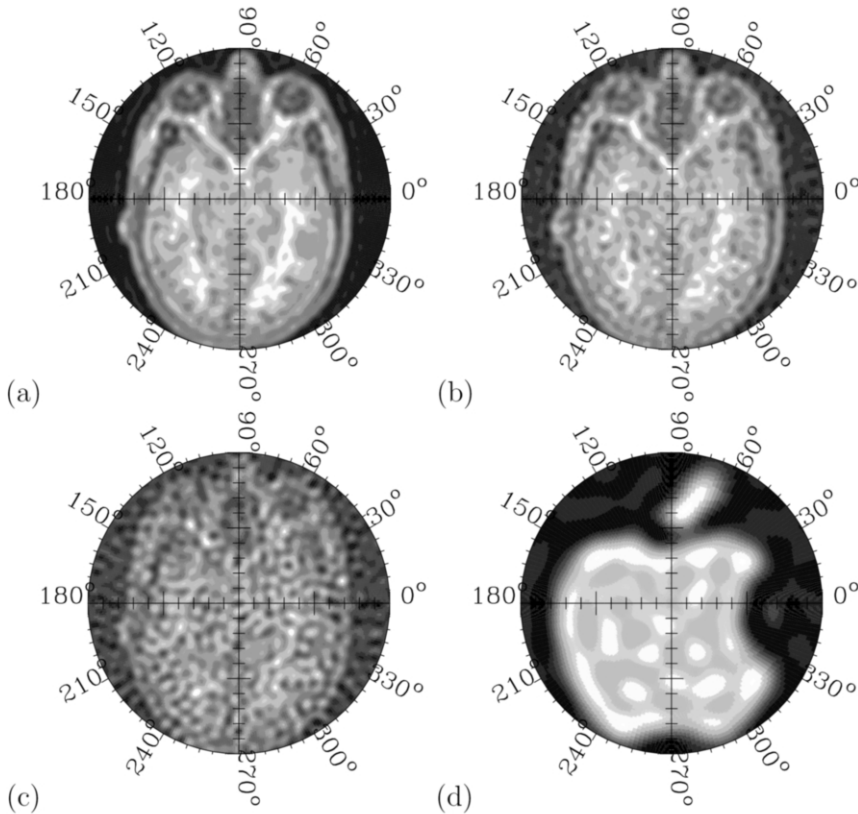


Fig. 4. Examples of quantized tomographic reconstructions. (a) Simulated QCT reconstruction of the brain slice of Fig. 3a, for  $5 \times 10^7$  data points using cutoff  $M = 300$  and  $\gamma = 1$ . (b) (c) Intermediate reconstructions from the previous simulation: in (b)  $5 \times 10^6$  data points have already been collected, in (c) only  $5 \times 10^5$  points have been collected. Using QCT, the reconstruction can be monitored while data is being gathered and the irradiation can be stopped when a sufficient level of detail has been reached. (d) Simulated QCT reconstruction of the apple-logo of Fig. 3b. For a simpler picture, much less data is necessary to obtain a good detail. Here only  $5 \times 10^5$  data were used, with  $M = 40$  and  $\gamma = 1$ .

from quadrature measurement results. This permits to recover a fake “density matrix”  $\rho$ , whose corresponding Wigner function is the sought tomogram.

How does the quantum state reconstruction procedure work in the case of a single harmonic oscillator? Here we sketch the main ideas and refer the interested reader to specific review articles on the subject [5].

The state of the harmonic oscillator can be obtained from the measurement

of the quadrature operator  $X_\phi$ . Varying  $\phi$ , the quadratures span a set of observables which are combinations of position  $Q$  and momentum  $P$ . In fact, they take the form  $X_\phi \equiv (a^\dagger e^{i\phi} + a e^{-i\phi})/2$ , where the annihilation operator  $a$  is defined as  $a \equiv Q + iP$ .<sup>7</sup> The quadrature observables can be measured via a homodyne detector, and the state of the oscillator can be recovered from the measurement results through homodyne tomography [7,6]. This procedure is based on the tomographic identity

$$(5) \quad \varrho = \int_{\mathbb{C}} \frac{d^2\lambda}{\pi} \text{Tr} \left[ \varrho e^{\lambda a^\dagger - \lambda^* a} \right] e^{\lambda^* a - \lambda a^\dagger},$$

where  $*$  denotes complex conjugation and the integration is performed on the whole complex plane [we use the compact notation  $d^2\lambda \equiv d\text{Re}(\lambda) d\text{Im}(\lambda)$ ]. There is no simple way to derive Eq. (5), even though it is a straightforward operatorial calculation. (It can be interpreted as an expansion of the density operator  $\varrho$  on a basis of displacement operators  $e^{\lambda^* a - \lambda a^\dagger}$  by recalling that the scalar product in a space of operators takes the Hilbert-Schmidt form  $\langle A|B \rangle = \text{Tr}[A^\dagger B]$ ). By writing the tomographic identity in polar coordinates  $\lambda = ir e^{i\phi}/2$ ,  $\varrho$  can be expressed in terms of quadrature operators as

$$(6) \quad \varrho = \int_0^\pi \frac{d\phi}{\pi} \int_{-\infty}^{+\infty} \frac{dr |r|}{4} \text{Tr} \left[ \varrho e^{irX_\phi} \right] e^{-irX_\phi}.$$

We can calculate the trace with a basis of quadrature eigenstates  $|x_\phi\rangle$  for every  $\phi$ , and take the matrix elements  $nm$  of both members in the Fock basis (by multiplying both members to the left by  $\langle n|$  and to the right by  $|m\rangle$ ). We get

$$(7) \quad \varrho_{nm} = \langle n|\varrho|m\rangle = \int_0^\pi \frac{d\phi}{\pi} \int_{-\infty}^{+\infty} dx_\phi \int_{-\infty}^{+\infty} \frac{dr |r|}{4} \langle x_\phi|\varrho|x_\phi\rangle \langle n|e^{-ir(X_\phi - x_\phi)}|m\rangle,$$

where  $x_\phi$  is the eigenvalue relative to the eigenstate  $|x_\phi\rangle$  of the quadrature  $X_\phi$ . From the Born statistical formula it follows that the term  $\langle x_\phi|\varrho|x_\phi\rangle$  in Eq. (7) is the probability that a measurement of the quadrature  $X_\phi$  on the state  $\varrho$  has a result  $x_\phi$ . Integrals which contain a probability  $p(x)$  can be easily evaluated

<sup>7</sup> The annihilation and creation operators have commutator  $[a, a^\dagger] = 1$ . When acting on a energy eigenstate  $|n\rangle$  of the oscillator, the annihilation operator  $a$  produces the eigenstate  $|n-1\rangle$  with one quantum less, whence its name. On the contrary, its hermitian conjugate operator  $a^\dagger$  (the “creation” operator) gives  $|n+1\rangle$ . The annihilation and creation operators respectively destroy and create an energy quantum (i.e. a photon, when the harmonic oscillator describes a quantized radiation field).

using Monte-Carlo integration as

$$(8) \quad \int dx p(x) F(x) = \lim_{N \rightarrow \infty} \frac{1}{N} \sum_{k=1}^N F(x_k),$$

where the  $N$  points  $x_k$  are distributed according to the probability  $p(x)$ . Thus, expressing the first two integrals of Eq. (7) in this form, we obtain the reconstruction procedure of Eq. (1), given that we define the kernel function as

$$(9) \quad K_{nm}(\phi, x) \equiv \int_{-\infty}^{+\infty} \frac{dr |r|}{4} \langle n | e^{-ir(X_\phi - x)} | m \rangle.$$

Expressing the quadrature  $X_\phi$  in terms of  $a$  and  $a^\dagger$ , it is straightforward (but not effortless) to obtain the expression of Eq. (2). This completes the proof of the density matrix reconstruction procedure. Notice that in this derivation we have applied the Born statistical formula. In principle, it is consistent only if we can give a probabilistic interpretation to the density matrix  $\rho$ . This requires some conditions on  $\rho$  (i.e. positivity and trace one normalization) that are not always met when we apply the QCT method, since we are treating the tomographic intensity profiles as if they were quantum measurement results. Nevertheless, as the simulations show, the QCT method is robust to non positivity of  $\rho$  (none of the density operators relative to the simulated reconstructions are positive with the chosen amplification parameter  $\gamma$ ). The same cannot be said for other reconstruction methods (such as the maximum likelihood which will be analyzed in the following section).

In order for the above procedure to be of any use we still need to connect the density operator  $\rho$  to the image we are seeking. This is done by interpreting the state's Wigner function  $W(x, y)$  as an image, i.e. by choosing the value of the image pixel at coordinates  $x, y$  according to the value of  $W(x, y)$ . A density matrix  $\rho$  can be put into one-to-one correspondence with a Wigner function through the following equations, for  $\alpha = x + iy$

$$(10) \quad W(x, y) \equiv \int_{\mathbb{C}} \frac{d^2\lambda}{\pi} \text{Tr} \left[ \rho e^{\lambda a^\dagger - \lambda^* a} \right] e^{\lambda \alpha^* - \lambda^* \alpha}$$

$$(11) \quad \rho = 2(-1)^{-a^\dagger a} \int_{\mathbb{C}} d^2\alpha W(x, y) e^{-2(\alpha a^\dagger - \alpha^* a)}.$$

The first of these is the definition of the Wigner function and can be seen as a functional form of the operator identity of Eq. (5). The second can be obtained employing the tomographic identity starting from the expression  $W(x, y) =$

$2\text{Tr} [\varrho e^{-2(\alpha a^\dagger - \alpha^* a)} (-1)^{a^\dagger a}] / \pi$ . Equation (3) follows straightforwardly from the definition (10), by evaluating the trace in the Fock basis  $|n\rangle$ , and performing the integration in polar coordinates  $r$  and  $\phi$ .

### 3 Possible future directions

In this section we analyze some of the possible refinements of the method detailed above. They are obtained in the same spirit of extending to classical tomography the methods developed for quantum state reconstruction, which is the leitmotif of this paper.

#### 3.1 Adaptive tomography

The kernel function that recovers the density matrix through the reconstruction of Eq. (1) is not unique. In fact, it is possible to add to each of the terms  $K_{nm}$  an arbitrary function of the data which has zero average. These are the so-called *null estimators*. The addition of a null estimator doesn't change the statistical averages—i. e. it gives the same results  $\varrho_{nm}$ —however it can change their variance. Thus, one can reduce the statistical noise by adding appropriate null functions suited to reducing the variance of the collected set of data. In homodyne tomography, the null estimators are functions of the form [9]

$$(12) \quad \mathcal{N}_n^\pm(\phi, x) = e^{\pm i(n+1)2\phi} g_\pm(x e^{i\phi}),$$

where  $n$  is a natural number, and both  $g_+$  and  $g_-$  are analytic functions on the complex plane. By choosing a suitable parametrization for these functions, it is possible to minimize the root-mean-square error of the experimental data using the least-squares method: we find an estimator for the density matrix which is less statistically noisy than the kernel  $K_{nm}$ . In Fig. 5 we present a striking example of the noise reduction that can be obtained through adaptive techniques in quantum tomographic reconstructions.

#### 3.2 Maximum likelihood

The maximum likelihood method is based on the assumption that the data we collect is the most probable. Suppose that  $p_\epsilon(x)$  is the probability of obtaining the datum  $x$  given the parameter  $\epsilon$  we want to estimate. The joint probability of obtaining the set of data  $\{x_i\}$  with  $i = 1, \dots, N$  is  $\prod_{i=1}^N p_\epsilon(x_i)$ . The maximum likelihood method consists in looking for the parameter  $\epsilon$  that maximizes this joint probability or, equivalently, its logarithm  $\mathcal{L}(\epsilon) = \sum_{i=1}^N \log p_\epsilon(x_i)$ .

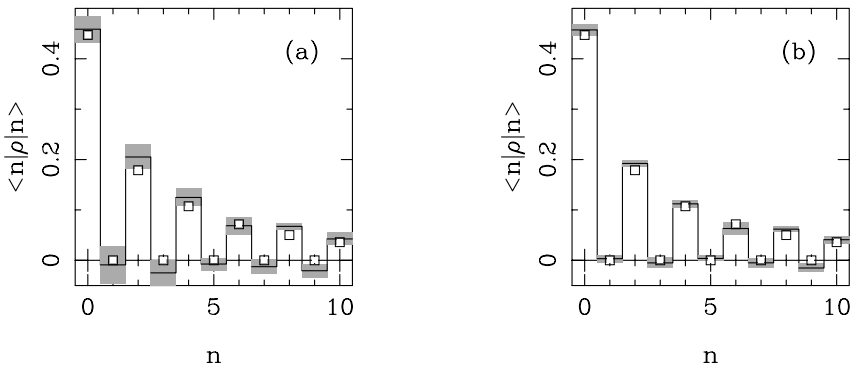


Fig. 5. Example (taken from Ref. [9]) of the statistical noise reduction obtained in quantum tomography using the adaptive noise reduction scheme. The same simulated experimental data have been treated in different ways. In the left graph, we simply averaged the pattern functions  $K_{mn}(\phi_k, x_k)$  of Eq. (1) on the data  $\{\phi_k, x_k\}$  to estimate the matrix elements (white squares) with their error bar (gray boxes). The black lines refer to the theoretical values. In the right graph, the same data is analyzed adding null functions  $\mathcal{N}(\phi_k, x_k)$  optimized on this set of data. Notice the drastic reduction in the statistical noise and the adaptation of the average values. (The simulation refers to the reconstruction of the diagonal matrix elements of a squeezed vacuum state.)

[The logarithm is introduced solely to convert the product into a summation and to avoid dealing with excessively small numbers]. The maximum likelihood method is the most statistically efficient estimation procedure: for a sufficiently large data set, the statistical error associated to the estimated quantities can achieve the Cramer-Rao bound, which is a lower bound to any estimation procedure [4].

In principle we can apply this method to the tomographic reconstruction without resorting to any “quantum trick”. In fact, the probability of each detection event is the marginal integral of the image (which gives the intensity profiles, see Fig. 1). Thus, choosing the maximum likelihood parameters  $\epsilon$  as the single image pixels, we could maximize the probability of obtaining the data we collected on the set of all possible images. This would give a very good estimation of the image itself, but it is evident that such a problem is numerically intractable even for the lowest quality images. In fact, to obtain an image with a resolution of  $500 \times 500$  pixels, we would have to maximize the function  $\mathcal{L}$  (which is a function of thousands or millions of data points) on a parameter space of dimension  $2.5 \times 10^5$ .

In the spirit of the present work, one could try to recover the density

matrix associated to the sought image, following the lines of the maximum likelihood state reconstruction [2]. Depending on the complexity of the image, good quality reconstructions can be obtained also for relatively small cut-off parameter  $M$ . This corresponds to a small number of parameters of  $\varrho$  to be estimated. However, as anticipated above, the probabilistic interpretation connected to the operator  $\varrho$  requires it to be positive: since we are boldly interpreting the intensity profiles of the tomogram as results of a quantum homodyne measurement, we cannot in general expect to recover a positive  $\varrho$ . (The “real” Wigner function of a quantum state must satisfy certain smoothness and normalization conditions, which arbitrary images do not satisfy.) The requirement of positivity is not necessary for the QCT method outlined in the previous sections, but it seems to be crucial for maximum likelihood, so that the reconstruction of an arbitrary Hermitian  $\varrho$  seems impossible via the maximum likelihood method. One may force the maximum search to positive  $\varrho$  artificially (e. g. using the Cholesky decomposition [2]), leading to the positive  $\varrho$  “nearest” (in some appropriately defined metric) to the  $\varrho$  corresponding to the sought image. The error introduced in the image will not be too big, provided that the actual image has density matrix with eigenvalues not too negative. When does this happen? The Heisenberg uncertainty relations translate into a lower bound for the product between variances of the marginal distributions of the Wigner function along two orthogonal directions. This means that, if we limit the analysis to positive  $\varrho$ , we will not be able to resolve small features in the image, i.e. smaller than a Heisenberg cell in phase space. The scale parameter  $\gamma$  introduced in Sec. 1 can be tuned to reduce the area of the Heisenberg cell of the the image, leading ultimately to a Heisenberg cell corresponding to a single image pixel, giving a positive  $\varrho$  for any image. Of course, in this case, there is no advantage in using the density matrix reconstruction since the state corresponding to such an amplified image will need a huge density matrix to be described. It may be still interesting to consider intermediate situations, however, due to the numerical burden for likelihood maximization, we have not analyzed this method further.

### 3.3 Other quantum tomographies

Up to now we have focused on adapting homodyne tomography to the classical imaging problem. Since there is a plethora of different quantum state reconstruction procedures for a huge number of different physical systems [10], one may ask whether other types of quantum tomographies may prove more apt to treat the intensity profiles coming from a classical tomographic detection

array. For example, it is conceivable that in the case in which the spatial resolution of the tomographic detectors is limited (yielding only a finite number of possible values for the parameter  $x$ ) the tomography of systems with finite degrees of freedom (e.g. spin systems) might provide better results. Other statistical methods are known that allow one to obtain the Wigner function directly from the homodyne data [1]: it is plausible they also might have applications in the imaging context. Finally it is conceivable that the methods described in this paper can be fruitfully extended also to the reconstruction of 3-dimensional images (starting from 2d or 1d intensity profiles) by adding an index to the recovered density matrix.

## 4 Conclusions

In conclusion we have presented a method to perform tomographic reconstructions based on the (easily parallelizable) reconstruction of a “density matrix” through appropriate averaging of functions of the outcomes of single-photon events at the tomographic detectors. The tomogram is then obtained from the density matrix through a simple numerical procedure. Not only the irradiation levels can be drastically decreased, but it is also possible to monitor in real time the reconstruction and interactively stop the irradiation as soon as a sufficient level of detail has been reached. The QCT method presented here is not optimal yet, and lines for further improvement have been also presented, which have a lot of potential and are worth further analysis.

## Acknowledgement

This work has been supported by the Italian Ministry of University and Research. We acknowledge A. Coppola for explaining to us the inner workings and the dosimetry of actual CT-scan devices.

## A Appendix. Factorized kernel functions

In this appendix we review the factorization of the kernel functions  $K_{nm}(\phi, x)$  of Eq. (2), which was first given in Ref. [14]. We follow the notation of Ref. [5]<sup>8</sup>. Although more involved, the factorized form presents the great advantage of being numerically fast and more stable, with the function  $K_{nm}(\phi, x)$  factorized into a product of two vectors: one dependent only on the index  $n$

---

<sup>8</sup> This notation differs from others because of a  $\sqrt{2}$  factor in the quadrature definition.

and the other only on  $m$ . Separate recursion relations are then available for both vectors, and are given here. We only provide the algorithm: for a proof of the equivalence of this kernel with the one of Eq. (2), we refer the reader to Refs. [14].

For  $m \geq n$ , the kernels  $K_{nm}$  can be factorized as

$$(A.1) \quad K_{nm}(\phi, x) = e^{i(m-n)\phi} \left[ x u_n(x) v_m(x) - \sqrt{n+1} u_{n+1}(x) v_m(x) - \sqrt{m+1} u_n(x) v_{m+1}(x) \right],$$

where  $u_j(x)$  and  $v_j(x)$  are defined by the following recursion relations (they are respectively the normalizable and unnormalizable wavefunctions of the harmonic oscillator relative to the  $j$ th eigenvalue). For  $n \geq m$ , on the other hand, we can use the fact that  $K_{nm} = K_{mn}$ . The recursion which defines  $u_j$  is

$$(A.2) \quad u_{-1}(x) = 0$$

$$(A.3) \quad u_0(x) = e^{-x^2}$$

$$(A.4) \quad u_j(x) = [2x u_{j-1}(x) - \sqrt{j-1} u_{j-2}(x)] / \sqrt{j}.$$

The recursion which defines  $v_j$  is the same as Eq. (A.4), but it is advisable to use it in the reverse order to avoid numerical instabilities since  $v_0$  is defined in terms of the imaginary error function which can have accuracy problems. Thus two different strategies are suggested, depending on the value of  $x$ . Define  $\alpha_j \equiv \sqrt{j+1}/2$ . If  $|x| < \alpha_{4M} - 1/2\alpha_{4M}^{-1/3}$  (where  $M$  is the cutoff parameter), we can employ the above recursion relation backwards, i.e.

$$(A.5) \quad v_{j-2}(x) = [2x v_{j-1}(x) - \sqrt{j} v_j(x)] / \sqrt{j-1},$$

starting from the asymptotic form of  $v_j$  valid for  $j \simeq 4M$ ,

$$(A.6) \quad v_j(x) = \frac{(8\pi)^{1/4}}{\sqrt{\alpha_j \sin \kappa_j}} \sin \left[ \frac{\alpha_j^2}{2} [\sin(2\kappa_j) - 2\kappa_j] + \pi/4 \right],$$

where  $\kappa_j \equiv \arccos(x/\alpha_j)$ . Otherwise, for  $|x| > \alpha_{4M} - 1/2\alpha_{4M}^{-1/3}$ , we can use the asymptotic form of  $v_j(x)$  for large  $x$ , i.e. the recursion

$$(A.7) \quad v_0(x) = e^{x^2}/x$$

$$(A.8) \quad v_j(x) = \frac{\sqrt{j}}{2x} v_{j-1}(x).$$

Even though analytically involved, the algorithmic implementation of the kernel functions with the expressions presented in this appendix is easy. The tomographic simulations presented in this paper are based on them.

## References

- [1] Artiles L. M., R. D. Gill, M. I. Guta, *An invitation to quantum tomography*, J. Royal Stat. Soc. B **67** (2005), 109-134.
- [2] Banaszek K., G. M. D'Ariano, M. G. A. Paris, and M. F. Sacchi, *Maximum-likelihood estimation of the density matrix*, Phys. Rev. A **61**, (2000) R10304.
- [3] Barrett H. H. and W. Swindell, "Radiological imaging : the theory of image formation detection and processing" vol. 2, Academic Press, New York, (1981).
- [4] Cramer H., "Mathematical Methods of Statistics", Princeton University Press, Princeton, (1946).
- [5] D'Ariano G. M., *Measuring quantum states*, in "Quantum Optics and the Spectroscopy of Solids", ed. by T. Hakioğlu and A.S. Shumovsky, Kluwer Academic Publishers (1997), p. 175.
- [6] D'Ariano G. M., U. Leonhardt, and H. Paul, *Homodyne detection of the density matrix of the radiation field*, Phys. Rev. A **52**, (1995) R1801-R1804.
- [7] D'Ariano G. M., C. Macchiavello, and M. G. A. Paris, *Detection of the density matrix through optical homodyne tomography without filtered back projection*, Phys. Rev. A **50**, (1994) 4298-4302.
- [8] D'Ariano G. M., C. Macchiavello, M. G. A. Paris, *A fictitious photons method for tomographic imaging*, Opt. Comm. **129** (1996), 6-12.
- [9] D'Ariano G. M. and M. G. A. Paris, *Adaptive quantum homodyne tomography*, Phys. Rev. A **60** (1999), 518-528; D'Ariano G. M. and M. G. A. Paris, *Optimized tomography of observables*, Acta Phys. Slov. **48** (1998), 191.
- [10] D'Ariano G. M., M. G. A. Paris, and M. F. Sacchi, *Quantum Tomography*, Advances in Imaging and Electron Physics **128** (2003), 205-308; D'Ariano G. M., M. G. A. Paris, and M. F. Sacchi, *Quantum tomographic methods*, in "Quantum State Estimation", Lecture Notes in Physics, vol. 649, Springer-Verlag, Berlin, (2004) p. 7-58.
- [11] Gradshteyn I. S., I. M. Ryzhik , "Table of integrals, series, and products", Academic Press, (1980), formulas 9.2471 and 8.9716.
- [12] Johns H. E., J. R. Cunningham "The physics of radiology", Charles C. Thomas Publisher, Springfield IL, (1983).
- [13] Leonhardt U. and M. Munroe, *Number of phases required to determine a quantum state in optical homodyne tomography*, Phys. Rev. A **54** (1996), 3682-3684.

- [14] Leonhardt U., M. Munroe, T. Kiss, Th. Richter, and M. G. Raymer, *Sampling of photon statistics and density matrix using homodyne detection*, Opt. Comm. **127** (1996), 144-160; G. M. D'Ariano, C. Macchiavello, and N. Sterpi, *Systematic and statistical errors in homodyne measurements of the density matrix*, Quantum Semiclass. Opt. **9** (1997), 929-940.
- [15] Mackay R. S., "Medical images and displays", J. Wiley & Sons, New York, (1984).
- [16] Natterer F., "The mathematics of Computerized Tomography", J. Wiley & Sons, New York, (1986).
- [17] Shapiro J., "Radiation protection: a guide for scientists and physicians", II Ed., Harvard University Press, Cambridge, (1990).
- [18] Technical manual of the GE Lightspeed plus tomographer; Department of health of the United Kingdom, Technical evaluation of the Philips MX8000 IDT (2004), available at <http://www.mhra.gov.uk>.
- [19] Vogel K. and H. Risken, *Determination of quasiprobability distributions in terms of probability distributions for the rotated quadrature phase*, Phys. Rev. A, **40** (1989), 2847-2849.